Biosensors and Bioelectronics 41 (2013) 84–89

Contents lists available at SciVerse ScienceDirect

Biosensors and Bioelectronics

journal homepage: www.elsevier.com/locate/bios

ZnO nanostructure-modified QCM for dynamic monitoring of cell adhesion and proliferation

Pavel Ivanoff Reyes [a], Ziqing Duan [a], Yicheng Lu [a,*], Dmitry Khavulya [b], Nada Boustany [b]

[a] Department of Electrical and Computer Engineering, Rutgers University, Piscataway, NJ 08854-8058, United States
[b] Department of Biomedical Engineering, Rutgers University, Piscataway, NJ 08854-8058, United States

ARTICLE INFO

Article history:
Received 11 April 2012
Received in revised form
2 July 2012
Accepted 21 July 2012
Available online 5 September 2012

Keywords:
Zinc oxide nanostructure
Quartz crystal microbalance
Cell monitoring

ABSTRACT

Noninvasive examination of live cell function in real-time is essential in advancing the understanding of the dynamic progression of cell's biological processes. We present a dynamic and noninvasive method of monitoring the adhesion and proliferation of bovine aortic endothelial cells (BAEC) using a ZnO nanostructure-modified quartz crystal microbalance (ZnOnano-QCM) biosensor. The ZnOnano-QCM biosensor consists of a conventional QCM with ZnO nanostructures directly grown on its sensing electrode deployed in-situ of a standard cell culture environment. Cell adhesion to the ZnO surfaces with various morphologies is studied and the optimal morphology is chosen for the BAEC adhesion. The ZnOnano-QCM biosensor displays enhanced sensitivity compared to the standard QCM sensor with ~10 times higher frequency shift and motional inductance, and ~4 times higher measured motional resistance at full confluency. The dynamic motional resistance and inductance relating to the cells' viscoelastic properties during growth are extracted from the measured time-evolving acoustic spectra. The Butterworth-Van-Dyck (BVD) model is adapted for the ZnOnano-QCM biosensor system and is used to correlate the measured time-evolving acoustic spectra with the motional characteristics of cell attachment and proliferation.

1. Introduction

Non-invasive and real-time examination of live cell function is essential in advancing the understanding of the mechanistic and dynamic progression of biological processes related to cell growth and death. Such understanding has a great impact on development of the cell-based drugs and assays. Standard methods such as optical microscopy, hemacytometry, and flow cytometry (Freshney, 2005) often involve invasively killing the cells and tagging them with optically active biomolecules to obtain information about their growth, proliferation, and function. Recently there is an increasing interest in using impedance spectrum analysis of acoustic wave devices such as the quartz crystal microbalance (QCM), the QCM with dissipation (QCM-D) for noninvasive and dynamic cell growth studies (Alessandrini et al., 2006; Fredriksson et al., 1998; Heitmann and Wegener, 2007; Li et al., 2005; Lord et al., 2006; Marx et al., 2005; Rodahl et al., 1997; Wegener et al., 1998; Zhou et al., 2000). The QCM which is a bulk acoustic wave device has been used as a compact, versatile and cost effective sensor with a high quality factor (Q), typically 10^4–10^6 at room temperature in vacuum or gaseous environment (Rodahl et al., 1995). QCM devices can operate in the range of several MHz to tens of MHz. The QCM-D on the other hand, is a modified version of the QCM which allows the sensor to simultaneously detect frequency shifts and energy dissipation (Fredriksson et al., 1998). For cell monitoring applications, the impedance spectrum analysis using the QCM and QCM-D sensors measure the frequency shift, and impedance as a function of time during the cell growth. In addition, the QCM-D measures time evolution of the acoustic energy dissipation due to cell activity. Such applications to cell growth analysis for cell-based drug assays and biophysical analysis were reported by Tan et al. (2009a, 2009b), Zhou et al. (2010), and Wegener et al. (2000).

ZnO is emerging as a wide bandgap semiconductor. Through proper doping and alloying ZnO can be made as a multifunctional material, which is particularly attractive for sensor technology. ZnO based sensors have demonstrated high sensitivity to CH_4, CO, H_2O, H_2, NH_3, trimethylamine, ethanol and NO_2 (Anisimkin et al., 1995; Hsueh et al., 2007). ZnO and its ternary alloy $Mg_xZn_{1-x}O$ are known to be the biocompatible oxides, in which Zn and Mg are important elements for neurotransmitter production and enzyme function (Miller and Trantim, 1998). ZnO nanostructures with different morphologies (nanometer-scale rods, belts, tips, etc.) can be grown on various substrates including Si, quartz, glass, and metals. ZnO nanostructures are also considered as a coating material for medical implants (Lee et al., 2008). It is shown that ZnO nanorods are compatible with intracellular material and are highly sensitive to pH changes inside cellular environments (Al-Hilli

* Corresponding author. Tel.: +1 732 445 3466; fax: +1 732 445 2820.
E-mail address: ylu@rci.rutgers.edu (Y. Lu).

0956-5663/$ - see front matter © 2012 Elsevier B.V. All rights reserved.
http://dx.doi.org/10.1016/j.bios.2012.07.039

et al., 2006). ZnO nanorods are also used for detection of enzymatic reactions with target biochemicals (Wei et al., 2006). The biocompatibility of ZnO and its feasibility for biosensing applications are further demonstrated in detections of proteins, antibodies, and DNA through the proper surface functionalizations (Reyes et al., 2009; Taratula et al., 2006; Zhang et al., 2007; Chen et al., 2009). The control of the surface wettability of ZnO nanotips between the super-hydrophillic and super-hydrophobic states is used to dramatically enhance the sensitivity of the biosensors and to reduce the consumption of the liquid samples (Zhang et al., 2007). The use of nanostructured ZnO for biological cell analysis has been mainly focused on (i) a nanostructured platform to facilitate cellular adhesion for various cell lines (Lee et al., 2008), (ii) a conductive nano-coating for intracellular probes mainly to detect cytoplasmic pH (Asif et al., 2009; Al-Hilli and Willander, 2009), and (iii) a material for enhancing optical detection (fluorescence and Raman type microscopy) (Adam and Dorfman et al., 2006; Dutta et al., 2009).

In this paper we present a novel cell monitoring technology which combines the unique sensing ability and biocompatibility of ZnO nanostructures with the dynamic and noninvasive measuring characteristics of QCM device to form the ZnO nanostructure-modified QCM sensor (ZnO_{nano}-QCM). In contrast with the reported methods, the ZnO_{nano}-QCM has ZnO nanostructures that serve as both of the biomolecular interface via surface functionalization and the sensitivity-enhancing layer resulting from the controlled morphology and giant effective surface area. This combination is expected to greatly enhance the device sensitivity, allow for simultaneous measurements of multiple parameters in a single test, and enable noninvasive and dynamic monitoring. The system features a portable and cost effective design. The biophysical properties, mainly viscoelastic transitions, mass accumulation, and cell adhesion and proliferation relating to cell activity are monitored in real-time through the sensor's specific time-evolving spectral signatures, including peak frequency shift, motional resistance and inductance. We adapted the Butterworth-Van-Dyck (BVD) model to correlate the measured spectral signals with the motional components of the ZnO_{nano}-QCM sensing system.

2. Material preparation and experimental procedures

2.1. Growth of ZnO with various surface morphologies

ZnO films of various surface morphologies were grown on 22 mm square glass cover slips and on the QCM and ZnO_{nano}-QCM by the metal-organic chemical vapor deposition (MOCVD) technique. Diethylzinc (DEZn) and ultra-high purity O_2 are used as the Zn precursor source and oxidizer, respectively. A chamber pressure of ~50 Torr was maintained during growth. Three different surface morphologies ("flat", "rough", and "sharp") were prepared (see Section 3.1) by varying the substrate temperature during MOCVD growth. The ZnO films were characterized using field emission scanning electron microscope (FESEM, Hitachi S-800), and the surface roughness was determined using the atomic force microscopy (AFM, Veeco Nanoscope Multimode). All samples and devices were sterilized with ethyl alcohol and distilled water and then treated with the human fibronectin (BD Biosciences, Bedford, MA) for 1 h. The samples were then placed in a standard 6-cell well and filled with cell medium for standard cell growth analysis.

2.2. Cell culture protocol

The cell line used for all experiments was bovine aortic epithelial cells (BAEC). All cells were maintained in the standard humidified incubator (5% CO_2 and 95% air) at 37 °C. The cells were grown in low glucose Dubelcco's modified eagle medium (DMEM) supplemented with 1% L-Glutamine, 1% bovine brain extract (BBE) (Clonetics, Inc.), 0.5% Heparin, 10% fetal bovine serum (FBS), and 0.4% of 10,000 U/ml penicillin and 10,000 mg/ml streptomycin solution. The cell culture was trypsinized and diluted for re-seeding after ~85% confluency was reached. The fibronectin solution was prepared using 1 mg of human fibronectin (BD Biosciences) diluted into 1 mL of PBS buffer solution.

Standard optical microscopy was used to confirm the cell growth on ZnO-on-glass samples, while fluorescence microscopy (Zeiss Axiovert 200 M, Gottingen, Germany) with a 548 nm filter and 576 nm excitation was used for the optically opaque devices. For the fluorescence microscopy the growth medium was modified with a living-cell tracer (Cell Tracker Orange CMRA) by preparing a 1:5 solution of CMRA fluorescent tracker and dimethyl sulfoxide (DMSO) to the growth medium.

2.3. Set-up of ZnOnano-QCM for the cell monitoring system

The schematic of a ZnO_{nano}-QCM device is shown in Fig. 1(a) for the top view, and in Fig. 1(b) for the cross sectional view of the multilayer structure. The piezoelectric AT-cut quartz layer is sandwiched between two 100 nm gold electrodes. The sensing area is 0.2047 cm^2. The ZnO_{nano}-QCM device consists of ZnO nanostructured films grown directly on a standard QCM through a shadow mask. The optimal ZnO nanostructure morphology was determined through the control of the MOCVD growth conditions described in Section 2.1. The ZnO nanostructure layer has thickness of ~500 nm. The ZnO-covered sensing area was exposed to UV light to make it super-hydrophilic (Zhang et al., 2007). The combined effect of giant surface area of the nanostructures and superhydrophilic state

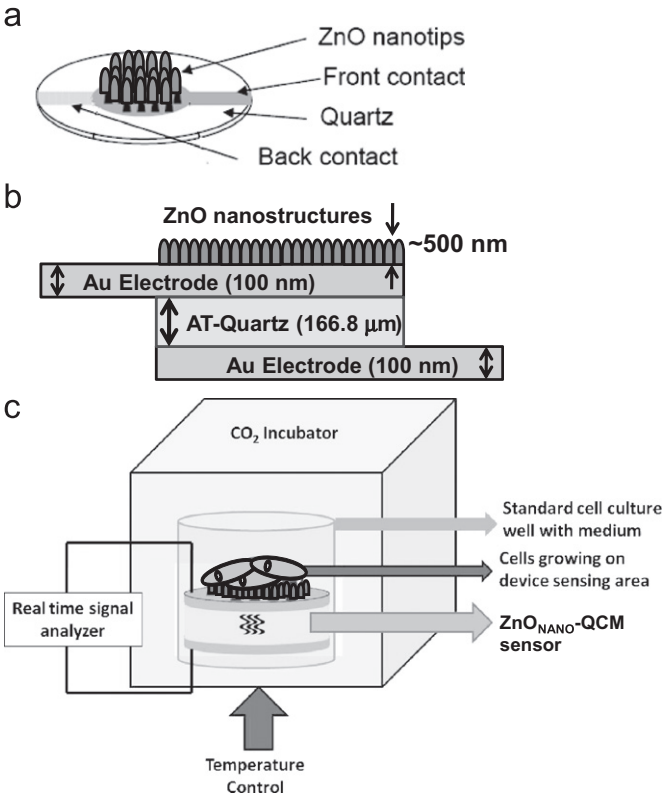

Fig. 1. (a) The ZnOnano-QCM biosensor schematic, (b) its multilayer (c) setup for deploying the ZnOnano-QCM biosensor for noninvasive and dynamic cell growth monitoring.

makes the ZnO_{nano}-QCM a very sensitive mass measuring, and viscoelastic monitoring device. The operating frequency of the standard QCM is 10 MHz, while the ZnO_{nano}-QCM has an operating frequency of 9.916 MHz.

The ZnO_{nano}-QCM was then sterilized and deployed inside a Teflon cell-growth well to serve as the test device (Fig. 1c), while a sterilized standard QCM was inserted in a similar Teflon cell-growth well to serve as the reference device. Both were filled with 50 μL of growth medium that was seeded with BAEC cells to have a $\sim 2 \times 10^5$ cells/mL concentration, and then placed in a standard CO_2 incubator for an average of 50 h.

2.4. Nano-QCM measurements and data analysis

The characterization and testing of the ZnOnano-QCM and standard QCM devices were conducted using an HP 8573D Network Analyzer (Agilent Technologies, Palo Alto, CA). The acoustic admittance (Y) spectrum of the device was automatically measured in every half-hour interval while the BAEC cells were growing on the ZnOnano-QCM sensor inside the incubator. The final output of the ZnOnano-QCM cell monitoring sensor is in the form of time-frequency 3D signals that contain multiple parameters in a single monitoring period, namely (i) peak frequency shift, (ii) motional resistance, (iii) motional inductance, and (iv) spectral shape evolution. Each of these parameters is analyzed for correspondence to the dynamic behavior of cell adhesion and proliferation and they are discussed in Section 3.2.

3. Results and discussion

3.1. Adhesion of BAEC Cells on ZnO surfaces with various morphologies

It is critical to determine the most suitable ZnO nanostructure morphology to facilitate the optimal adhesion of the cells to the device. In order to determine the optimum morphology for the cell adhesion, ZnO nanostructures with three different surface morphologies were grown as described in Section 2.1 and images are found in the supplementary materials Fig. S1(a–h). It was found that the substrate temperature played the major role on achieving various surface morphologies of ZnO films. Fig. S1(a–c) shows three different surface morphologies of ZnO films, taken by FESEM. The "flat" sample, shown in Fig. S1(a), was grown at a low temperature of $\sim$250 °C, while the "rough" sample (Fig. S1b) was grown at $\sim$330 °C. The "sharp" sample (Fig. S1c), required a relatively high temperature ($>$400 °C) for growth. The surface roughness (root mean square) of ZnO films was characterized by AFM, which is 1.39 nm for "flat" ZnO (Fig. S1a), 7.48 nm for "rough" (Fig. S1b) and 11.4 nm for "sharp" (Fig. S1c) sample. The samples were prepared for cell culture as discussed in Section 2.1. After 50 h the three samples were analyzed. For the flat ZnO surface, the cell culture is close to 100% confluency and uniformly spreading and proliferating on the ZnO substrate (Fig. S1d). However, it is found that after the entire duration of the monitoring cycle the cells have crowded with each other, competing for nutrients and space. This condition will eventually induce the cells to die and detach from the ZnO surface. On the other hand, the cells on the rough ZnO surface have reached about 75% confluency, uniform proliferation, and the individual cells have considerable amount of spreading as shown in Fig. S1(e). The cells adhered to the sharp ZnO surface, but did not establish good focal adhesion to facilitate uniform proliferation and proper individual cell spreading. The cell culture on the sharp ZnO surface only attained 40% confluency and a clumped cell distribution as shown in Fig. S1(f). This clumped distribution could cause localized areas on the ZnO surface where cell death is induced. The results of poor cell adhesion on sharp nanorods are consistent with the observation reported by Lee et al. wherein the same cell line (BAEC cells) lacked the ability to establish strong initial adhesion to the sharp nanostructures, thus prohibited them to produce lamellipodia (cell-anchoring mechanism). It would be a natural choice to use the flat ZnO surface since it gives us a large yield in cell growth, however, there is an inherent tradeoff in choosing the optimal ZnO morphology for the sensing surface. In terms of cell attachment, the cells favor the adhesion to flatter surfaces, but in terms of device performance the sharper surface provides the highest sensitivity due to the large effective sensing area provided by the nanostructures (Reyes et al., 2009; Zhang et al., 2007). It is determined that the rough ZnO surface is the most suitable morphology for adhesion and viability for cell growth without sacrificing the device sensitivity.

For the comparison, we repeated the same cell adhesion experiment on two different ZnOnano-QCM sensors; one with the rough ZnO surface and another with the sharp ZnO surface, both grown on the top electrode. Fig. S1(g) and (h) shows the fluorescence images of the living cells on the ZnO_{nano}-QCM with sharp and rough surface, respectively. The fluorescence micrograph representing the ZnO_{nano}-QCM with the sharp surface shows low cell attachment and proliferation whereas the one with the rough surface shows uniform cell proliferation, good attachment and individual cell spreading.

3.2. Cell monitoring using ZnO_{nano}-QCM

The ZnO_{nano}-QCM device with the optimized ZnO surface morphology (rough ZnO surface) was utilized to monitor adhesion and proliferation of the cells. The control (standard QCM) and test (ZnO_{nano}-QCM) devices were set up as described in Section 2.3. The devices were seeded with cell density that would be fully confluent in approximately 45–50 h. While the cells were growing on each device, we continuously measured the sensor's admittance parameter $Y(\omega)$ for half-hour intervals.

The time-evolving resonance frequency shift $\delta f(t) = f_0 - f(t)$ of both devices were monitored, where f_0 is the resonant frequency of the device right after it has been injected with the cell-seeded medium and $f(t)$ is the subsequent resonant frequency of the device after a time t. Fig. 2 shows the plot of $\delta f(t)$ for both devices. The most evident feature of this plot is the enhanced sensitivity of the ZnO_{nano}-QCM over the standard QCM where the maximum frequency shift at confluence of the ZnO_{nano}-QCM is $\sim$10 times larger than the standard QCM. This can be attributed to the giant effective surface area made available for cell attachment to the ZnO nanostructures on the sensing area of the ZnO_{nano}-QCM device. According to (Heitmann and Wegener, 2007), the detectable activity of cell growth on the QCM-type devices only happens at the interface of the cells and the sensing area. Adding the ZnO nanostructures to the QCM sensing area enhances this interfacial interaction by providing a huge effective sensing area for the device. The ZnO_{nano}-QCM device also exhibits a linear cell proliferation from initial seeding before it tapers off at 40 h when the cells reach full confluency. The standard QCM on the other hand shows nonlinear proliferation rate (Fig. 2 inset) and reaches confluency early at 25 h of incubation. Moreover, the fluorescence images of both the devices taken after 50 h (Fig. 3a and b) show that the cell culture reached similar full confluency on both devices.

We need to establish the correspondence between the time-evolving admittance measurements from the ZnO_{nano}-QCM (which is an electrical parameter) with the mechanical parameters at the sensing area. The transmission line model of the basic QCM outlined by Bandey et al. (1997) was used to show the correspondence. The

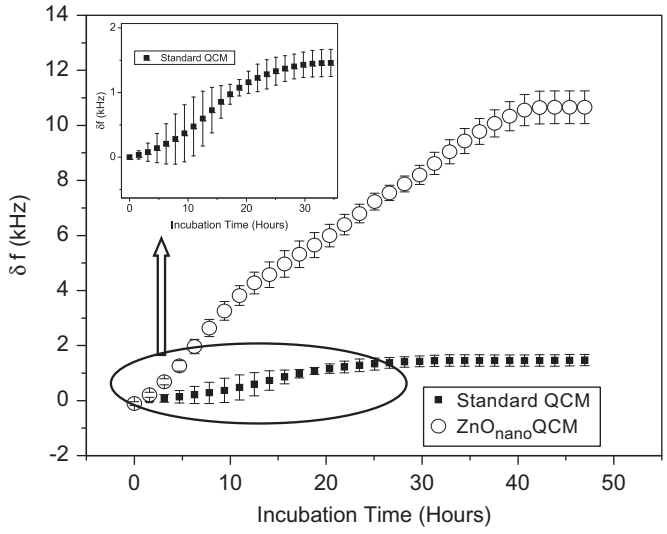

Fig. 2. The time-evolving frequency shift (deviation from resonance frequency) for the standard QCM (solid squares), and the ZnOnano-QCM (open circles) showing ~10 times enhanced sensing performance by the ZnOnano-QCM.

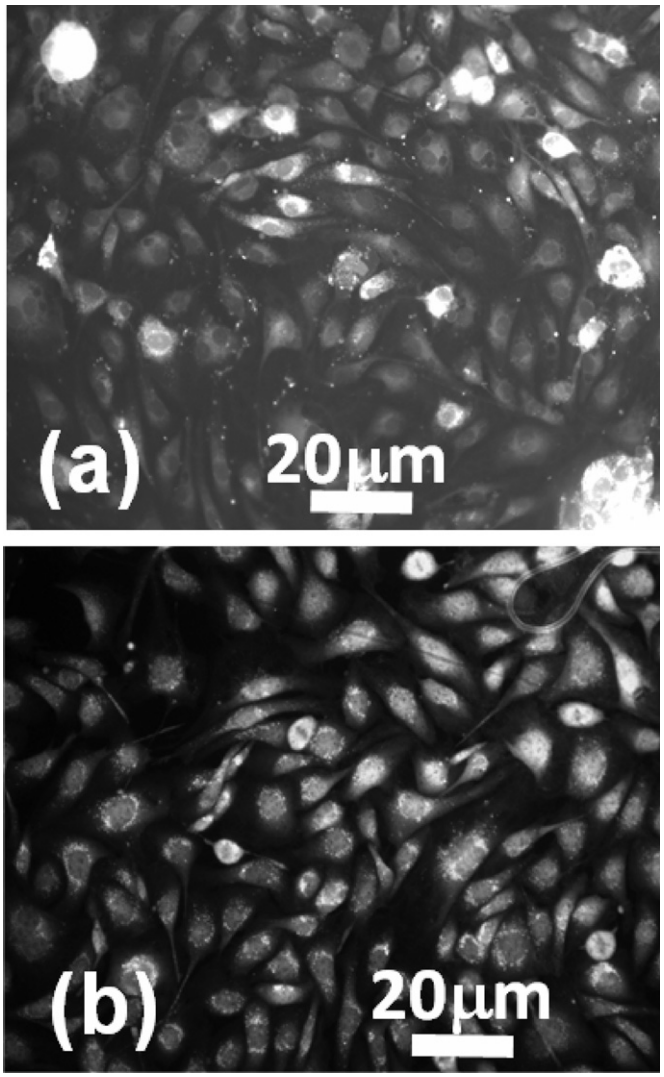

Fig. 3. (a) 20× fluorescence image of the BAEC cells on the standard QCM after full confluency; (b) 20× fluorescence image of the BAEC cell on the ZnOnano-QCM sensing after full confluency.

model is adapted to our cell monitoring system which consists of four mechanical transmission line impedance layers as depicted in Fig. 4(a): (i) the basic QCM layer described by its characteristic impedance Z_Q and the coupling coefficient of quartz K^2, (ii) the ZnO nanostructure layer modeled as an ideal rigid mass layer described by the ZnO density ρ_{ZnO}, (iii) the biological cell layer modeled as a finite thickness viscoelastic film described by the cell density ρ_{cell} and the complex shear modulus $\mathbf{G}_{cell}$, and (iv) the cell growth medium modeled as a semi-infinite Newtonian fluid described by its density ρ_{medium} and viscosity coefficient η_{medium}. Layer (i) is treated as the basic device, and layers (ii)–(iv) are mechanical load impedances. If a small-load assumption is used, i.e. total load density is less than 5 mg/cm^2 and the total viscosity is less than 10^3 g^2/cm^4 s, then the entire transmission line model can be simplified into a lumped-parameter circuit equivalent called the Butterworth-Van-Dyke (BVD) lumped-parameter model (Bandey et al., 1997; Wegener et al., 2000). This assumption is also valid for cell growth (Wegener et al., 2000). The BVD equivalent circuit of the nano-QCM is shown in Fig. 4(b), which is composed of a RLC circuit in series with a load impedance Z_{Load} (which includes the contribution due to the ZnO nanostructure, cell layer, and the growth medium), and in parallel with a capacitor C_0. C_0 describes the basic characteristics of the basic QCM far from the resonance frequency. The branch of the circuit that represents the motional characteristics of the nano-QCM near and at the resonance frequency is the load impedance with the series RLC circuit, composed of R_{QCM}, L_{QCM}, and C_{QCM}, the motional resistance, inductance and capacitance of the quartz resonator at no load, respectively. When the basic QCM experiences mechanical perturbations due to a collective load placed on its sensing electrode, the load impedance Z_{Load} takes effect. The load impedance can be further represented by a series RLC circuit (R_{Load}, L_{Load}, and C_{Load}) and is given by

$$Z_{Load} = R_{Load} + j\omega_0 L_{Load} \frac{1}{j\omega_0 C_{Load}} \tag{1}$$

where ω_o is the resonant frequency of the device. The motional capacitance is exclusively dependent on the material properties and dimensions of the quartz crystal (Wegener et al., 2000), thus C_{Load} can be lumped together with C_{QCM}. The electrical parameter (Z_{Load}) is directly related to the mechanical impedance experienced by the acoustic wave due to the physical perturbations occurring at the attached overlaying material given by the expression (Wegener et al., 2000):

$$Z_{Load} = \frac{1}{Y_{Load}} = \frac{\pi}{4K^2\omega_0 C_0} \frac{Z_{mechL}}{Z_{QCM}} \tag{2}$$

where K^2 is the coupling coefficient of the piezoelectric quartz layer, Z_{mechL} is the mechanical impedance due to the ZnO layer+cellular layer+growth medium attached to the sensing area, and Z_{QCM} is the impedance the QCM at no load. Eqs. (2) and (3) give the expression for R_{Load} and L_{Load} and are related to the measured admittance parameter by

$$R_{Load} = \frac{\pi}{4K^2\omega_0 C_0} \frac{\mathrm{Re}\{Z_{mechL}\}}{Z_{QCM}} = \frac{\mathrm{Re}\{Y_{Load}\}}{\mathrm{Re}^2\{Y_{Load}\} + \mathrm{Im}^2\{Y_{Load}\}} \tag{3}$$

$$L_{Load} = \frac{\pi}{4K^2\omega_0 C_0} \frac{\mathrm{Im}\{Z_{mechL}\}}{Z_{QCM}} = \frac{-\mathrm{Im}\{Y_{Load}\}}{\omega_0(\mathrm{Re}^2\{Y_{Load}\} + \mathrm{Im}^2\{Y_{Load}\})} \tag{4}$$

The quantity R_{Load} corresponds directly to the mechanical or motional resistance and designates dissipation of acoustic energy due to the attached cell growth layer on the nano-QCM surface. The parameter L_{Load} on the other hand is directly proportional to the stored energy by the cell layer (i.e. elasticity increase). Y_{Load} is the measured admittance spectrum minus the no-load admittance spectrum of the standard QCM. Adapting our cell monitoring setup to the Z_{mechL} expression developed by (Bandey et al., 1997), the mechanical

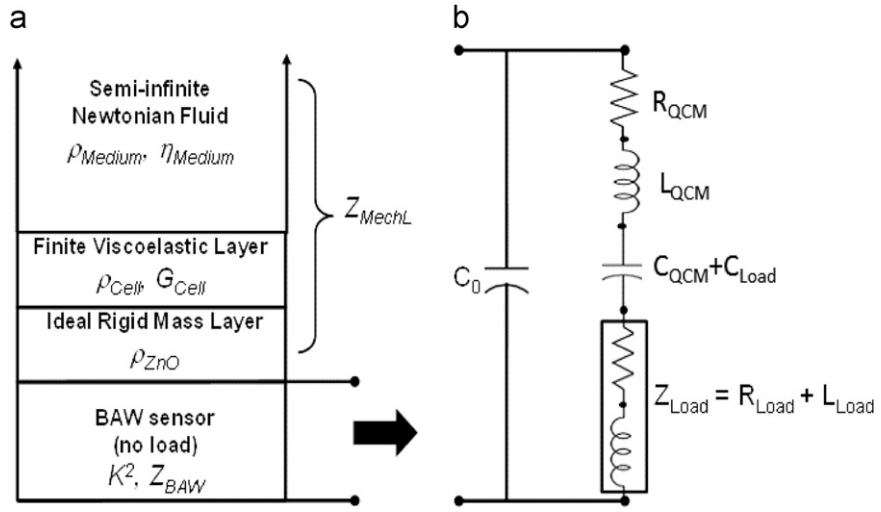

Fig. 4. (a) The mechanical impedance model of the ZnOnano-QCM cell monitoring system, (b) the corresponding electrical circuit model of the ZnOnano-QCM cell monitoring system.

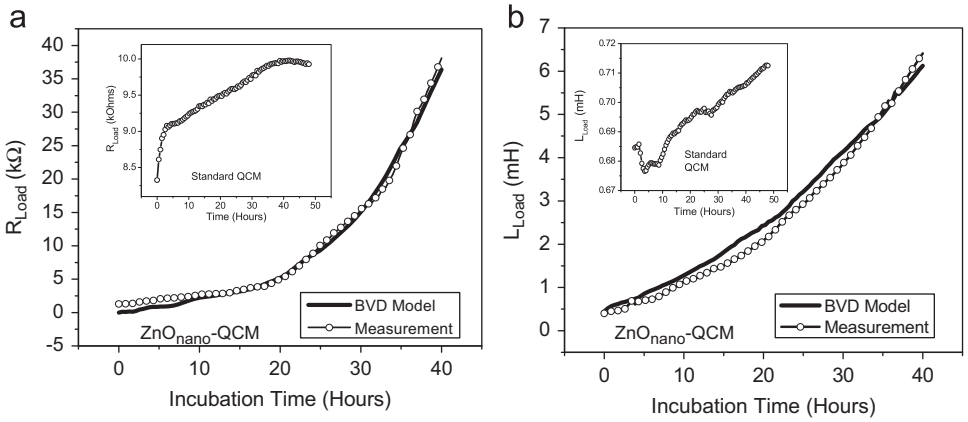

Fig. 5. (a) The time-evolving load resistance of the ZnOnano-QCM due to the adhering and proliferating cells and inset: the load resistance change in the standard QCM; (b) the time-evolving load inductance of the ZnOnano-QCM and inset: the load inductance change in the standard QCM.

impedance becomes a combination of the mechanical effects derived from the mechanical model in Fig. 5(a) and is given by Eq. (5)

$$Z_{MechL} = j\omega\rho_{ZnO} + Z_{cell}\left[\frac{Z_{Medium}\cosh(\gamma_{cell}h_{cell}) + Z_{cell}\sinh(\gamma_{cell}h_{cell})}{Z_{cell}\cosh(\gamma_{cell}h_{cell}) + Z_{Medium}\sinh(\gamma_{cell}h_{cell})}\right] \quad (5)$$

where $j\omega\rho_{ZnO}$ represents the impedance of the rigid ideal mass ZnO nanostructured layer, $Z_{Cell} = \rho_{Cell}\mathbf{G}_{Cell}$ is the impedance of the finite-thickness (h_{cell}) viscoelastic cell layer, and Z_{medium} is the impedance of the growth medium as a semi-infinite Newtonian fluid, which is given by

$$Z_{Medium} = (1+j)\sqrt{\left(\frac{\omega\rho_{Medium}\eta_{Medium}}{2}\right)} \quad (6)$$

To isolate the effects of the ZnO layer and the growth medium (and also obtain empirical values for the BVD parameters for these layers) we measured the admittance parameter of the ZnO_{nano}-QCM right after the ZnO nanostructure deposition on the sensing electrode to show that the only effect the ZnO film, the growth medium and fibronectin layers collectively does on the signal is to introduce a Sauerbrey frequency shift (Fig. S2(a) and (b) of supplementary materials) This means that the this collective layer does not contribute to the dynamic transitions occurring in the cell monitoring setup. These will serve as the baseline signals which verify that the changes we observed in the time-evolving admittance spectra are only due to the viscoelastic cell layer.

We used Eqs. (3) and (4) to generate the motional resistance and inductance plots that relate the measured admittance spectra to the viscoelastic changes happening during the cell growth process monitored by the ZnO_{nano}-QCM. Fig. 5(a) shows the motional resistance of the ZnO_{nano}-QCM for the 40-h cell growth monitoring period. The inset shows the same parameter for the standard QCM. The most obvious information derived here is the highly enhanced sensitivity of the ZnO_{nano}-QCM compared to a standard QCM in detecting viscoelastic transition. For the standard QCM, the total change in motional resistance ΔR_{total} was only 1.5 kΩ, while for the ZnO_{nano}-QCM it was 37.5 kΩ which is 25 times higher than the standard QCM. Fig. 5(b) shows the motional inductance experienced by the nano-QCM due to the cell growth. Fig. 5(a) and (b) reveals certain details about the cell growth on the ZnO_{nano}-QCM sensor. L_{Load} increases continuously from 0 to 40 h while R_{Load} changes in different time intervals. From 0 to 16 h R_{Load} increases slowly from 1.29 kΩ to 3.84 kΩ. This indicates a small energy dissipation due to the low value of R_{Load}. This may be due to the onset of proliferation on the sensing area. For the time interval 16–30 h there is a rapid increase in the value of R_{Load} indicating a high energy dissipation that may be caused by the formation of more rigid focal adhesion points by the individual cells, and the increase of cell spreading. At 30–40 h the

value of R_{Load} further increases faster indicating further energy dissipation due to onset of full confluency or cell crowding. This increase in energy dissipation is caused by the dampening of the shear waves induced by the large amount of cellular proliferation. Fig. S3 (supplementary materials) shows a plot of the motional resistance versus motional reactance. The upward curvature $\partial^2 R_{Load}/\partial(\omega L_{Load})^2 > 0$ indicates that the energy loss per unit mass of the cells increases with the cell culture proliferation. The solid lines in Fig. 5(a) and (b) represent the BVD fitting curves derived from empirical parameter fitting of the individual layers in the BVD model. The BVD model curves agree with the measured parameters; however, they do not closely fit, especially in the early stages of cell growth because of the limitations intrinsic to the BVD model. The assumption in the model is that the cells have a constant density and have a uniform distribution on the entire sensing area. This model therefore approaches higher accuracy as confluency is reached rather than in the early proliferation stage.

4. Conclusion

The integration of ZnO nanostructures and a standard QCM forms a surface-modified QCM biosensor (nano-QCM), which possesses significantly enhanced sensitivity over the conventional QCM counterpart. The nano-QCM biosensor is installed in situ using a standard cell culture environment for noninvasive and dynamic cellular monitoring. We have demonstrated the controlled adhesion and proliferation of BAEC cells on the nanostructured ZnO surface with the optimized surface morphology. The ZnOnano-QCM exhibited enhanced sensitivity to detection of cell adhesion, proliferation, and viscoelastic transitions through a single measurement of time-frequency 3D acoustic spectra. The ZnOnano-QCM shows 10 times increased sensitivity in frequency shift due to total cell proliferation in comparison with the standard QCM. The Butterworth-Van-Dyke (BVD) lumped-parameter model analysis was applied to the measured acoustic spectra to extract dynamic information from the signal's spectral shape evolution, peak frequency shift, and amplitude modulation. The presented technology provides a base for noninvasive, real-time, dynamic and label-free cellular monitoring.

Appendix A. Supplementary material

Supplementary data associated with this article can be found in the online version at http://dx.doi.org/10.1016/j.bios.2012.07.039.

References

Adam Dorfman, Nitin, Kumar, Hahm, Jong-in, 2006. Langmuir 22, 4890–4895.
Alessandrini, A., Croce, M.A., Tiozzo, R., Facci, P., 2006. Applied Physics Letters 88, 083905.
Al-Hilli, S.M., Al-Mofarji, R.T., Willander, M., 2006. Applied Physics Letters 89 (17), 173119.
Al-Hilli, S., Willander, M., 2009. Nanotechnology 20, 175103.
Anisimkin, V.I., Penza, M., Valentini, A., Quaranta, F., Vasanelli, L., 1995. Sensors and Actuators B: Chemical 23 (2–3), 197–201.
Asif, M.H., Fulati, A., Nur, O., Willander, M., Brännmark, C., Strålfors, P., Börjesson, S.I., Elinder, F., 2009. Applied Physics Letters 95, 023703.
Bandey, H., Hillman, A.R., Brown, M.J., Martin, S.J., 1997. Faraday Discussions 107, 105–121.
Chen, Y., Reyes, P.I., Duan, Z., Saraf, G., Wittstruck, R., Lu, Y., Taratula, O., Galoppini, E., 2009. Journal of Electronic Materials 38 (8), 1605–1611.
Dutta, R., Sharma, P., Pandey, A., 2009. Digest Journal of Nanomaterials and Biostructures 4 (1), 83–87.
Fredriksson, C., Kihlman, S., Rodahl, M., Kasemo, B., 1998. Langmuir 14, 248–251.
Freshney, R.I., 2005. Culture of Animal Cells: A Manual of Basic Techniques, 5th ed. Wiley.
Heitmann, V., Wegener, J., 2007. Analytical Chemistry 79, 3392–3400.
Hsueh, T.-J., Chang, S.-J., Hsu, C.-L., Lin, Y.-R., Chen, I.-C., 2007. Applied Physics Letters 91, 053111.
Li, J., Thielmann, C., Reuning, U., Johannsmann, D., 2005. Biosensors & Bioelectronics 20, 1333–1340.
Lee, J., Kang, B.S., Hicks, B., Chancellor Jr., T.F., Chu, B.H., Wang, H.–T., Keselowsky, B.G., Rena, F., Lele, T.P., 2008. Biomaterials 29, 3743–3749.
Lord, M.S., Modin, C., Foss, M., Duch, M., Simmons, A., Pedersen, F.S., Milthorpe, F., Besenbacher, B.K., 2006. Biomaterials 27, 4529–4537.
Marx, K.A., Zhou, T., Montrone, A., McIntosh, D., Brauhut, S.J., 2005. Analytical Biochemistry 343, 23–34.
Miller, B.G., Trantim, T.W., 1998. Journal of the American Chemical Society 120, 2666.
Reyes, P.I., Zhang, Z., Chen, H., Duan, Z., Zhong, J., Saraf, G., Lu, Y., Taratula, O., Galoppini, E., Boustany, N.N., 2009. IEEE Sensors Journal 10 (10), 1302–1307.
Rodahl, M., Höök, F., Fredriksson, C., Keller, C.A., Krozer, A., Brzezinski, P., Voinova, M., Kasemo, B., 1997. Faraday Discussions 107, 229–246.
Rodahl, M., Höök, F., Krozer, A., Brzezinski, P., Kasemo, B., 1995. The Review of Scientific Instruments 66 (7), 3924–3930.
Tan, L., Xie, Q., Jia, X., Guo, M., Zhang, Y., Tang, H., Yao, S., 2009a. Biosensors & Bioelectronics 24 (6), 1603–1609a.
Tan, L., Jia, X.E., Jiang, X.F., Zhang, Y.Y., Tang, H., Yao, S.Z., Xie, Q.J., 2009b. Biosensors & Bioelectronics 24 (7), 2268–2272b.
Taratula, O., Galoppini, E., Wang, D., Chu, D., Zhang, Z., Chen, H., Saraf, G., Lu, Y., 2006. The Journal of Physical Chemistry B 110 (13), 6506–6515.
Wegener, J., Seebach, J., Janshoff, A., Galla, H.-J., 2000. Biophysical Journal 78, 2821–2833.
Wegener, J., Janshoff, A., Galla, H.-J., 1998. European Biophysics Journal 28, 26–37.
Wei, A., Sun, X.W., Wang, J.X., Lei, Y., Cai, X.P., Li, C.M., Dong, Z.L., Huang, W., 2006. Applied Physics Letters 89 (12), 123902.
Zhang, Z., Chen, H., Zhong, J., Saraf, G., Lu, Y., 2007. Journal of Electronic Materials 36 (8), 895.
Zhou, Y.P., Jia, X.E., Tan, L., Xie, Q.J., Lei, L.H., Yao, S.Z., 2010. Biosensors & Bioelectronics 25 (5), 1116–1121.
Zhou, T., Marx, K., Warren, M., Schulze, H., Braunhut, S., 2000. Biotechnology Progress 16, 268–277.